Substituted 3-styryl-2-pyrazoline Derivatives as an Antimalaria: Synthesis, *in vitro* Assay, Molecular Docking, Druglikeness Analysis, and ADMET Prediction

(Penggantian Terbitan 3-styryl-2-pyrazoline sebagai Antimalaria: Sintesis, Asai *in vitro,* Dok Molekul, Analisis Keserupaan Dadah dan Ramalan ADMET)

Linda Ekawati[1], Beta Achromi Nurohmah[1], Jufrizal Syahri[2] & Bambang Purwono[1,*]

[1]Department of Chemistry, Faculty of Mathematics and Natural Science, Universitas Gadjah Mada, Jalan Kaliurang Sekip Utara Bulaksumur 21, Yogyakarta, 55281 Indonesia
[2]Department of Chemistry, Faculty of Mathematics and Natural Sciences, Universitas Muhammadiyah Riau, Jalan Tuanku Tambusai Ujung Nomor 1, Pekanbaru Indonesia

ABSTRACT

The synthesis, *in vitro* antimalarial assay, molecular docking, drug-likeness analysis, and ADMET prediction of substituted 3-styryl-2-pyrazoline derivatives as antimalaria have been conducted. The synthesis of N-phenyl (**1a–3a**) and N-acetyl-substituted (**1b–3b**) 3-styryl-2-pyrazolines was carried out using dibenzalacetone derivatives and hydrazine hydrate or phenylhydrazine. An *in vitro* antimalarial assay was conducted against the chloroquine-sensitive *Plasmodium falciparum* 3D7 strain, while molecular docking was performed toward the crystal protein of *Plasmodium falciparum* dihydrofolate reductase-thymidylate synthase (*Pf*DHFR-TS) (PDB ID: 1J3I). Furthermore, the prediction of drug-like properties was determined by assessing Lipinski's rules, and the pharmacokinetic parameters were also studied *in-silico,* including absorption, distribution, metabolism, excretion, and toxicity (ADMET). The *in vitro* assay showed that **3a** (IC$_{50}$ 0.101 µM) has excellent antimalarial activity, followed by **2a** (0.177 µM), and **1b** (0.258 µM). Molecular docking has supported the *in vitro* assay by showing the lowest CDOCKER energy for **3a** (–56.316 kcal/mol), then **2a** (–51.2603 kcal/mol), and **1b** (–48.8774 kcal/mol). The drug-like properties showed that all of the prepared compounds were acceptable based on Lipinski's rules and predicted to be potentially orally bioavailable. The ADMET analysis provided information that **3a** and **2a** could be proposed as the best lead antimalarial drugs with further modification to reduce the lipophilicity and toxicity properties.

Keywords: ADMET; antimalarial; dibenzalacetone; molecular docking; pyrazoline

ABSTRAK

Sintesis, asai antimalaria *in vitro*, dok molekul, analisis keserupaan dadah dan ramalan ADMET bagi terbitan 3-styryl-2-pyrazoline yang digantikan sebagai antimalaria telah dijalankan. Sintesis N-fenil (**1a–3a**) dan N-acetyl-substituted (**1b–3b**) 3-styryl-2-pyrazolines telah dijalankan menggunakan terbitan dibenzalaseton dan hidrazina hidrat atau fenilhidrazina. Ujian antimalaria *in vitro* telah dijalankan terhadap strain *Plasmodium falciparum* 3D7 yang sensitif terhadap klorokuin, manakala dok molekul dilakukan ke arah protein kristal *Plasmodium falciparum* dihidrofolat reduktase-timidilat sintase (*Pf*DHFR-TS) (PDB ID: 1J3I). Tambahan pula, ramalan sifat seperti ubat ditentukan dengan menilai peraturan Lipinski dan parameter farmakokinetik juga dikaji secara *in siliko*, termasuk penyerapan, pengedaran, metabolisme, perkumuhan dan ketoksikan (ADMET). Ujian *in vitro* menunjukkan bahawa **3a** (IC$_{50}$ 0.101 µM) mempunyai aktiviti antimalaria yang sangat baik, diikuti oleh **2a** (0.177 µM), dan **1b** (0.258 µM). Dok molekul telah menyokong ujian *in vitro* dengan menunjukkan tenaga CDOCKER terendah untuk **3a** (–56.316 kcal/mol), kemudian **2a** (–51.2603 kcal/mol) dan **1b** (–48.8774 kcal/mol). Sifat keserupaan dadah menunjukkan bahawa semua sebatian yang disediakan boleh diterima berdasarkan peraturan Lipinski dan diramalkan berpotensi bio tersedia secara oral. Analisis ADMET memberikan maklumat bahawa **3a** dan **2a** boleh dicadangkan sebagai ubat antimalaria terbaik dengan pengubahsuaian selanjutnya untuk mengurangkan sifat lipofilis dan ketoksikan.

Kata kunci: ADMET; antimalaria; dibenzalaseton; dok molekul; pirazolin

INTRODUCTION

Malaria is an infectious disease caused by plasmodium parasites, with an estimated 229 million cases in 2019 in 87 malaria-endemic countries (WHO 2020). According to the World Health Organization (WHO), the mortality rate has reached 409,000 cases in 2019, with 67% of total deaths among children under five years old (WHO 2020). To combat this disease, therapeutic use of antimalarial agents such as antifolate, quinoline, and artemisinin derivatives has been applied (Adebayo et al. 2020; Belete 2020). However, some studies have reported the occurrence of resistance and also diminished efficacy of the current antimalarial drugs (Adebayo et al. 2020; Belete 2020; Leroy 2017; WHO 2020). The resistance for antimalarial drugs is a serious problem in the eradication of malaria worldwide. Therefore, it is needed to discover and develop compounds with better antimalarial activity and new mechanisms of action (Tse et al. 2019).

The administration of a single antimalarial drug is considered weak in the treatment of malaria. For instance, chloroquine, as the commonly used antimalarial drug, has lost its efficacy due to resistance to *P. falciparum* (Ibrahim et al. 2020). Therefore, combination therapy, such as Artemisinin-based combination therapy (ACT), has been developed to overcome the efficacy problem. The ACT is used by combining a fast-acting artemisinin derivative with a slow-acting drug from another class compound in the therapy (Nigam et al. 2019). Changes in the combination might help to overcome the drug resistance problems.

Modification of the compounds structure is other attempts to develop new antimalarial agents. Modification of functional groups or substituents in the molecules must be considered to affect bioactivity. Heterocyclic compounds containing nitrogen, oxygen, and sulphur are being considered in the development of antiplasmodial drugs (Chugh et al. 2020). Pyrazolines as a five-membered ring heterocycle have been studied as antimalarial agents (Ekawati et al. 2020; Kalaria et al. 2018). Pyrazoline can be obtained from the cyclization reaction of dibenzalacetone derivatives (Aher et al. 2011). Although some symmetrical dibenzalacetone (1,5-diphenyl-1,4-pentadien-3-one) derivatives have been reported as antimalarial agents (Aher et al. 2011; Manohar et al. 2013), cyclization to pyrazoline could preserve antimalarial activities and reduce toxicity (Charris et al. 2019; Pandey et al. 2016).

Our previous study proposed that some 3-styryl-2-pyrazolines have heme polymerization inhibitory activity (Ekawati et al. 2020). In this present work, some substituted 3-styryl-2-pyrazolines from methoxy substituted-dibenzalacetone derivatives have been synthesized and tested *in vitro* antiplasmodial assay against the chloroquine (CQ)-sensitive *P. falciparum* 3D7 strain. The methoxy group is reported as an important substituent in some antimalarial drug candidates (Purwono et al. 2021; Septiana et al. 2022). The methoxy groups at the phenyl rings in the pyrazoline moieties could interfere with the apoptosis and initiate the destruction of *P. falciparum* DNA (Sharma et al. 2012; Wanare et al. 2010), and also exhibit excellent inhibitors of β-hematin formation (Charris et al. 2019; Chugh et al. 2020).

This work also presented molecular docking simulations on the crystal protein of the wild–type *Plasmodium falciparum* dihydrofolate reductase–thymidylate synthase (*Pf*-DHFR-TS) with a PDB ID of 1J3I to understand the interactions and binding affinity with the drug candidate compounds. Prediction of the drug-likeness and pharmacokinetic parameters (absorption, distribution, metabolism, excretion, and toxicity/ADMET) of the prepared compounds were also studied to understand their drug properties.

MATERIALS AND METHODS

The chemicals used in this investigation were benzaldehyde, 4-methoxy benzaldehyde, 3,4-dimethoxybenzaldehyde, ethanol, acetone, phenylhydrazine, hydrazine hydrate (80% in water), sodium hydroxide (NaOH), glacial acetic acid, hydrochloric acid (37%), n-hexane, and ethyl acetate (as eluents for thin-layer chromatography/TLC). All chemicals in the analytical grade were purchased from Merck and utilized without any further purification.

INSTRUMENTATION

The melting point was determined in open capillary tubes using an Electrothermal 9100 device (uncorrected). Fourier Transform Infra-Red (FTIR) spectra were obtained from Shimadzu-Prestige 21 (KBr pellet), while Gas chromatography (GC) and mass spectra (MS) were acquired from the Shimadzu QP-2100 spectrometer. The ^{1}H and ^{13}C-NMR spectra were recorded from JEOL JNM ECZ500R/S1 (500 MHz for ^{1}H, and 125 MHz for ^{13}C-NMR) with tetramethylsilane (TMS) as reference.

GENERAL PROCEDURE FOR THE SYNTHESIS OF SUBSTITUTED-DIBENZALACETONES (**1-3**)

The synthesis of dibenzalacetone derivatives **1-3** was carried out following the same procedure as in the previous

work (Ekawati et al. 2020). Acetone (5 mmol) was added gradually to a stirred solution of benzaldehyde or 4-methoxy benzaldehyde or 3,4-dimethoxy benzaldehyde (10 mmol) in 20 mL of ethanol at 1-4 °C. The mixture was further stirred for another 15 minutes in an ice bath to maintain a temperature of 1-4 °C. Afterward, 20 mL of sodium hydroxide solution (20%) was added dropwise while stirring, and the mixture was stirred for 1 hour. After the completion of the reaction (monitored by TLC using n-hexane: ethyl acetate, 1:1), the reaction mixture was neutralized with HCl solution (10%), and the solid product was filtered, washed with distilled water, dried, and recrystallized from ethanol. The structure of the purified product was then analyzed using FT-IR, GC- or DI-MS, and ^{1}H-NMR spectrometers.

(1E,4E)-1,5-bis(4-methoxyphenyl)penta-1,4-dien-3-one (2)

Yellow solid, 70.75%, m.p 121-123 °C (Lit. 121-124 °C, Wang et al. 2011). FTIR KBr (υ_{max}, cm^{-1}): 3017 (Csp^2 –H stretching), 2963 (Csp^3 –H stretching), 1628 (C=O α,β-unsaturated ketone), 1512 (aromatic C=C stretching), 1250 and 1034 (C–O ether), 980 (HC=CH trans). ^{1}H-NMR (500 MHz, CDCl$_3$) δ (ppm): 3.84 (6H, s, –OCH$_3$), 6.93 (2H, d, J = 9 Hz, H-Ar), 6.97 (1H, s, CH=CH), 7.56 (2H, d, J = 9 Hz, H-Ar), 7.70 (1H, d, J = 16 Hz, CH=CH). MS (EI, m/z): 294 (M$^+$, base peak), 186, 133, 121, 89, and 77.

GENERAL PROCEDURE FOR THE SYNTHESIS OF N-PHENYL PYRAZOLINES (1a-3a)

The preparation of N-phenyl pyrazolines **1a-3a** was performed according to the procedure in the previous work (Ekawati et al. 2020). Dibenzalacetones **1-3** (2 mmol) were dissolved in 15 mL of glacial acetic acid in a three-necked flask and were added with phenylhydrazine (2 mmol). The reaction mixture was refluxed for 8-11 h. After completion of the reaction (monitored using TLC with n-hexane: ethyl acetate, 1:1), the mixture was cooled down to room temperature and poured into iced distilled water. The precipitated product was then filtered, washed with distilled water, dried, and recrystallized with ethanol to give the desired compounds **1a-3a**. The structures of N-phenyl pyrazolines **1a-3a** were determined using FT-IR, GC- or DI-MS, ^{1}H-, and ^{13}C-NMR spectrometers.

(E)-5-(4-methoxyphenyl)-3-(4-methoxystyryl)-1-phenyl-4,5-dihydro-1H-pyrazole (2a)

Brick red solid, 88.31%, m.p 141- 143 °C (Lit. 140-141 °C, Nauduri & Reddy 1998). FTIR (υ_{max}, cm^{-1}): 3017 (Csp^2 –H stretching), 2924 (Csp^3 –H stretching), 1597 (C=N), 1458 (aromatic C=C stretching), 1319 (C–N), 1250 (C-O), and 949 (HC=CH trans). ^{1}H-NMR (500 MHz, DMSO-d$_6$) δ (ppm): 2.92 (1H, dd, J = 15 and 5 Hz, –CH$_2$), 3.67 (1H, d, J = 15 Hz, –CH$_2$), 3.70 (3H, s, -OCH$_3$), 3.76 (3H, s, -OCH$_3$), 5.39 (1H, dd, J = 10 and 5 Hz, –CH), 6.69 (3H, m, H-Ar), 6.90 (2H, m, H-Ar), 6.95 (4H, m, H-Ar), 7.10 (1H, d, J = 11 Hz, CH=CH), 7.14 (2H, m, H-Ar), 7.22 (1H, d, J = 11 Hz, CH=CH), 7.53 (2H, m, H-Ar). ^{13}C-NMR (125 MHz, DMSO-d$_6$) δ (ppm): 42.1 (–CH$_2$), 55.2 (-OCH$_3$), 62.2 (–CH), 113.7 (C-Ar), 118.5 (CH=CH), 119.2-133.1 (C-Ar), 134.6 (CH=CH), 149.3 (C=N), 159 (C-Ar). DI-MS (EI, m/z): 384, 159, 121, 91 (base peak), and 77.

GENERAL PROCEDURE FOR THE SYNTHESIS OF N-ACETYL PYRAZOLINE (1b-3b)

Three N-acetyl pyrazolines **1b–3b** were prepared with a modification of the procedure of compound **1a–3a**. Dibenzalacetone **1–3** (2 mmol) was reacted with hydrazine hydrate (2 mmol) in glacial acetic acid (10 mL) in reflux conditions for 7-11 h and monitored using TLC (with n-hexane: ethyl acetate, 1:1). The reaction mixture was cooled to room temperature and then poured into iced distilled water. The precipitate formed was then filtered, washed with distilled water, dried, and recrystallized with ethanol to give the desired N-acetyl pyrazoline compounds **1b–3b**.

(E)-1-(5-phenyl-3-styryl-4,5-dihydro-1H-pyrazol-1-yl) ethanone (1b)

Brown solid, 73.27%, m.p 121-124 °C. FTIR (υ_{max}, cm^{-1}): 3024 (Csp^2 –H stretching), 2924 (Csp^3 –H stretching), 1666 (C=O), 1558 (C=N), 1420 (aromatic C=C stretching), 1327 and 1142 (C–N), 957 (HC=CH trans). ^{1}H-NMR (500 MHz, DMSO-d$_6$) δ (ppm): 2.67 (3H, s, -CH$_3$), 3.33 (1H, dd, J = 17 and 5 Hz, –CH$_2$), 3.9 (1H, dd, J = 17 and 12 Hz, – CH$_2$), 5.84 (1H, dd, J = 12 and 5 Hz, -CH), 7.06 (1H, d, J = 16 Hz, CH=C**H**), 7.42 (1H, d, J = 16 Hz, C**H**=CH), 7.51 (2H, d, J = 8 Hz, H-Ar), 7.56 (1H, t, J = 4 Hz, H-Ar), 7.65 (1H, m, H-Ar), 7.67 (2H, t, J = 7 Hz, H-Ar), 7.77 (1H, t, J = 7 Hz, H-Ar). ^{13}C-NMR (125 MHz, DMSO-d$_6$) δ (ppm): 21.6 (–CH$_3$), 41.0 (–CH$_2$), 59.7 (-CH), 120.5 (CH=CH), 125.4 (C-Ar), 126.9 (C-Ar), 127.5 (C-Ar), 128.8 (C-Ar), 129.0 (C-Ar), 135.5 (C-Ar), 137.2 (CH=CH), 141.6 (C-Ar), 154.9 (C=N), 168 (C=O). GC-MS (EI, m/z): 290 (M$^+$), 247, 115, 91, 77, and 43 (base peak).

(E)-1-(5-(4-methoxyphenyl)-3-(4- methoxystyryl)-4,5-dihydro-1H-pyrazol-1-yl)ethanone (**2b**)

White solid, 77.14%, m.p 152-153 °C. FTIR (υ_{max}, cm^{-1}): 2924 (Csp^3 –H stretching), 1651 (C=O), 1605 (C=N), 1512 (C=C aliphatic), 1458 (aromatic C=C stretching), 1250 (C-O ether), 1335 and 1173 (C–N), 957 (HC=CH trans). ^{1}H-NMR (500 MHz, DMSO-d$_6$) δ (ppm): 2.34 (3H, s, -CH$_3$), 3.04 (1H, dd, J = 20 and 5 Hz, –CH$_2$), 3.54 (1H, dd, J = 20 and 10 Hz, – CH$_2$), 3.77 (3H, s, -OCH$_3$), 3.83 (3H, s, -OCH$_3$), 5.47 (1H, dd, J = 10 and 5 Hz, -CH), 6.72 (1H, d, J = 16 Hz, CH=C**H**), 6.84 (2H, m, H-Ar), 6.89 (2H, m, H-Ar), 6.98 (1H, d, J = 16 Hz, C**H**=CH), 7.14 (2H, m, H-Ar), 7.43 (2H, m, H-Ar). ^{13}C-NMR (125 MHz, DMSO-d$_6$) δ (ppm): 22.1 (–CH$_3$), 41.2 (–CH$_2$), 55.4 (-OCH$_3$), 55.5 (-OCH$_3$), 59.3 (-CH), 114.4 (C-Ar), 114.5 (C-Ar), 118.7 (CH=CH), 127.0 (C-Ar), 128.6 (C-Ar), 134.3 (C-Ar), 137.1 (CH=CH), 155.5 (C=N), 159.1 (C-Ar), 160.6 (C-Ar), 168.6 (C=O). DI-MS (EI, *m/z*): 350 (M$^+$), 307, 187, 121, 91, 77, and 43 (base peak).

(E)-1-(5-(3,4-dimethoxyphenyl)-3-(3,4-dimethoxystyryl)-4,5-dihydro-1H-pyrazol-1-yl) ethanone (**3b**)

White solid, 56.10%, m.p 171-172 °C. FTIR (υ_{max}, cm^{-1}): 2932 (Csp^3 –H stretching), 1659 (C=O), 1597 (C=N), 1512 (C=C aliphatic), 1450 (aromatic C=C stretching), 1265 (C-O ether), 1327 and 1142 (C–N), 956 (HC=CH trans). ^{1}H-NMR (500 MHz, DMSO-d$_6$) δ (ppm): 2.62 (3H, s, -CH$_3$), 3.31 (1H, dd, J = 15 and 5 Hz, –CH$_2$), 3.85 (1H, dd, J = 15 and 10 Hz, – CH$_2$), 4.13 (3H, s, -OCH$_3$), 4.15 (3H, s, -OCH$_3$), 4.20 (6H, s, -OCH$_3$), 5.77 (1H, dd, J = 10 and 5 Hz, -CH), 7.01 (1H, d, J = 11 Hz, CH=C**H**), 7.03 (1H, d, J = 5 Hz, H-Ar), 7.05 (1H, d, J = 2 Hz, H-Ar), 7.09 (1H, d, J = 8 Hz, H-Ar), 7.14 (1H, d, J = 5 Hz, H-Ar), 7.29 (1H, d, J = 11 Hz, C**H**=CH), 7.33 (1H, d, J = 5 Hz, H-Ar), 7.55 (1H, s, H-Ar). ^{13}C-NMR (125 MHz, DMSO-d$_6$) δ (ppm): 21.9 (–CH$_3$), 41.0 (–CH$_2$), 55.8 (-OCH$_3$), 59.4 (-CH), 108.5 (C-Ar), 108.8 (C-Ar), 111 (C-Ar), 111.3 (CH=CH), 117.4 (C-Ar), 118.5 (C-Ar), 121.1 (C-Ar), 128.6 (C-Ar), 134.4 (C=N), 135.2 (CH=CH), 148.4 (C-Ar), 149.1 (C-Ar), 149.7 (C-Ar), 150.1 (C-Ar), 155.2 (C=N), 168.4 (C=O). DI-MS (EI, *m/z*): 410 (M$^+$), 367 (base peak), 203, 151, 91, 77, and 43.

in vitro ANTIMALARIAL ACTIVITY ASSAY

An *in vitro* antimalarial activity assay was conducted following the previous work by Syahri et al. (2020a) with modification at the concentration of the samples. This assay was tested against the chloroquine-sensitive *P. falciparum 3D7* strain by microscopic evaluation of Giemsa-stained thin blood smears. The test compounds were dissolved in DMSO and then diluted into serial concentrations to obtain a final concentration of 1000, 100, 10, 1, and 0.1 µg/mL. Each sample solution (2 µL) was then transferred to 96-well microtiter plates and 198 µL of parasite suspension with a parasitemia level of ± 1% and a hematocrit of 5% was added to reach a final concentration of 10, 1, 0.1, 0.01, and 0.001 µg/mL. After incubation at 37 °C for 48 h, the culture was collected, and a thin blood film was made with 10% Giemsa's stain for microscopic examination. This assay was conducted with two replications for each sample.

The percentage of inhibition was calculated based on the formula: 100% – (% parasite growth in test solution/% parasite growth in negative control) × 100%), where the percentage of parasite growth was calculated from the number of infected erythrocytes for every 1,000 normal erythrocytes. Statistical analysis of the antimalarial activity (IC$_{50}$ value) was determined using Probit log analysis in SPSS 20.0 based on the percentage of inhibition data and the concentration of the tested compound. The classification of the antimalarial activity was decided according to the following criteria: very active, IC$_{50}$ < 1 µg/mL; active, IC$_{50}$ = 1-15 µg/mL; moderately active, IC$_{50}$ = 15-25 µg/mL; weakly active, IC$_{50}$ = 25-50 µg/mL; inactive, IC$_{50}$ > 50 µg/mL (de Souza et al. 2018), whereas Batista et al. (2009) classified antimalarial activity (IC$_{50}$) as excellent (< 1 µM); good (1-20 µM); moderate (20-100 µM); low (100-200 µM); and inactive (> 200 µM).

MOLECULAR DOCKING

Molecular docking was performed following previous procedures by Syahri et al. (2020b). The protein target was the crystal structure of the wild-type *Plasmodium falciparum* dihydrofolate reductase-thymidylate synthase (*Pf*DHFR-TS) protein with a PDB ID of 1J3I. The Re-docking step to the co-crystal ligand WR99210 resulted in an RMSD of 0.6542 Å. Interactions formed between the ligand and protein were then visualized using Discovery Studio Visualizer software.

PREDICTION OF DRUG-LIKENESS AND ADMET PARAMETERS

Prediction of the drug-like properties and ADMET parameters was performed by drawing the structure of the prepared compounds into an online web server named ADMETlab 2.0 (https://admetmesh.scbdd.com/

service/evaluation/index) (Xiong et al. 2021). The drug-like properties of the compounds were predicted based on Lipinski's rule of 5, where molecules with two or more violations of the rules would theoretically become unacceptable orally bioavailable as drugs. The rule takes into account several factors, including molecular weight ($\leq$ 500), number of hydrogen bonds donor ($\leq$5), number of hydrogen bonds acceptor ($\leq$ 10), and the partition coefficient (logP) (<5) (Lipinski et al. 2001).

The absorption of drugs was generated by membrane permeability (shown by colon cancer cell line/Caco-2), human intestinal absorption (HIA), P-glycoprotein inhibitor, P-glycoprotein substrate, and human oral bioavailability ($F_{20\%}$ and $F_{30\%}$) indicators. The Caco-2 permeability (as the log cm/s) is classified as excellent if the log unit is > –5.15. Meanwhile, the other parameters are grouped as either positive (category 1/+++) or negative (category 0/– – –).

The drug distributions were assessed based on the plasma protein binding (PBB), blood-brain barrier (BBB), and volume distribution (VD). The plasma protein binding is generated in percentage (%) with the empirical decision $\leq$ 90% is excellent, otherwise it is poor. In addition, the BBB parameter is divided into positive (category 1/+++) and negative (category 0/– – –). Furthermore, the empirical decision of the VD value is between 0.04 and 20 L/kg (excellent), and otherwise, it is poor.

The drug metabolism was predicted based on the profiles of the Cytochrome P450 (CYP) isozymes, such as CYP1A2, CYP2C19, CYP2C9, CYP2D6, and CYP3A4. This parameter is categorized into category 1 (substrate or inhibitor) and category 0 (non-substrate or non-inhibitor). The output value represents the probability of being substrate or inhibitor, ranging from 0 (– – –) to 1 (+++). The drug excretion was predicted based on the total clearance and the half-life (t½). The predicted total clearance is classified as low (< 5 mL/min/kg), moderate (5-15 mL/min/kg), or high (> 15 mL/min/kg), with the empirical decision that $\geq$ 5 is excellent and < 5 is poor. In addition, the half-life is classified as category 0 (short half-life with t½ < 3h) and category 1 (long half-life with t½ $\geq$ 3h) whereas the output value is the probability to have a long half-life, within the range of 0 to 1.

The toxicity was predicted by evaluating the hERG (human *Ether-à-go-go*-related gene) blockers, human hepatotoxicity (H-HT), rat oral acute toxicity, Ames toxicity, carcinogenicity, and drug-induced liver injury (DILI). All toxicity parameters are categorized

as negative (category 0/– – –) and positive (category 1/+++). The tested compounds with at least one positive endpoint in the predicted toxicity parameters are considered toxic (Dong et al. 2018).

RESULTS AND DISCUSSION

This work reported the preparation of symmetrical dibenzalacetones (**1–3**) via Claisen-Schmidt condensation of aryl aldehydes and acetone in a ratio of 2:1. Some of N-phenyl pyrazolines **1a–3a** and N-acetyl pyrazolines **1b–3b** were also prepared by the cyclo-condensation reaction of dibenzalacetone derivatives (**1–3**) with hydrazine hydrate or phenylhydrazine (Scheme 1).

The structures of all of the prepared compounds were elucidated and confirmed using spectroscopy methods such as FT-IR, GC– or DI–MS, ^{1}H-, and ^{13}C-NMR (see the Supplementary Data). The formation of pyrazoline can be mainly characterized from the ^{1}H-NMR spectra by observing the presence of doublet of doublets peak around 2.9 to 5 ppm from the two protons (–CH$_2$) in the pyrazoline ring. The ^{1}H-NMR spectra also recorded *trans* isomers of the respected pyrazolines by the *J* coupling of alkene groups (–CH=CH–) in the range of 11–16 Hz.

ANTIMALARIAL ACTIVITY ASSAY

In vitro antimalarial of six pyrazolines from dibenzalacetone against *P. faciparum* 3D7 atrain (CQ sensitive) is presented in Table 1. Excellent antimalarial activity (IC_{50} < 1µM) was exhibited by **3a**, followed by **2a** and **1b** with IC_{50} values of 0.101, 0.177, and 0.258 µM, respectively. In addition, compounds **1a**, **2b**, and **3b** were categorized to have good antimalarial activity with IC_{50} values in the range of 1 to 20 µM (Batista et al. 2009). These results are still higher than the IC_{50} of chloroquine as a standard drug, but they are remarkable potential for combination antimalarial therapy.

These results indicated that the presence of methoxy groups in N-phenyl pyrazolines **2a** and **3a** (IC_{50} = 0.177 and 0.101 µM) increased significantly the antimalarial activity than N-phenyl pyrazoline **1a** (IC_{50} = 2.937 µM). Inversely, the methoxy-substituted N-acetyl pyrazolines **2b** and **3b** (IC_{50} = 2.156 and 5.695 µM) have lower activities than pyrazoline **1b** (0.258 µM). The methoxy and N-phenyl substituents of pyrazolines **2a** and **3a** have better antimalarial activities than the corresponding methoxy and N-acetyl-substituted pyrazolines **2b** and **3b.** This result means that the number

of methoxy groups could increase the antimalarial activity of the N-phenyl substituted pyrazolines. However, the N-acetyl substituted pyrazoline **1b** has better antimalarial activity than N-acetyl substituted pyrazoline **1a**.
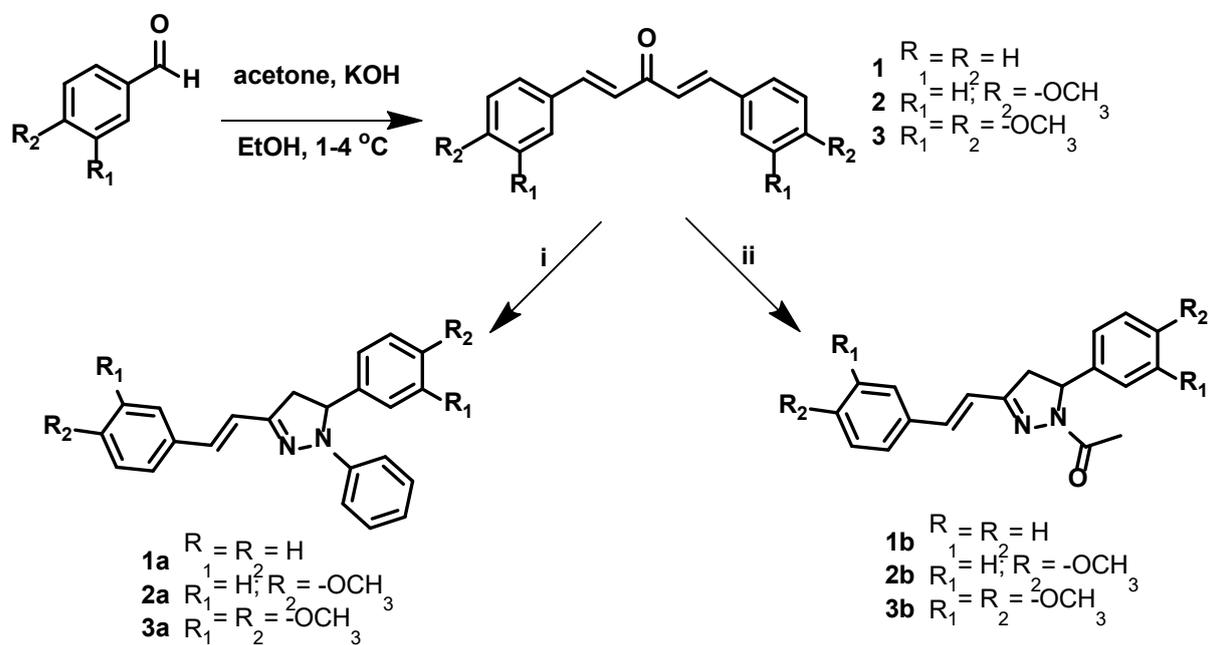
SCHEME 1. Synthesis of N-phenyl (**1a–3a**) and N-acetyl (**1b–3b**) pyrazolines from dibenzalacetones (**1–3**). i) phenylhydrazine, glacial acetic acid, reflux 8 h; ii) hydrazine hydrate (80% in H_2O), glacial acetic acid, reflux 7-11 h

TABLE 1. *In vitro* antimalarial activity of N-phenyl and N-acetyl substituted pyrazolines

Compounds	IC_{50} (μg/mL)	IC_{50} (μM)
1a	0.952 ±0.004	2.937 ± 0.013
2a	0.068 ± 0.016	0.177 ± 0.042
3a	0.045 ± 0.009	0.101 ± 0.020
1b	0.075 ± 0.001	0.258 ± 0.005
2b	0.755 ± 0.028	2.156 ± 0.079
3b	2.336 ± 0.078	5.695 ± 0.191
CQ	0.02	0.063

MOLECULAR DOCKING STUDIES

Molecular docking was performed to provide the prediction of binding modes and interactions formed between the compounds and the crystal protein 1j3I. pdb. The results of the *in-silico* studies are summarized in Table 2.

TABLE 2. Docking energy (CDOCKER) and interactions of N-phenyl (**1a**–**3a**) and N-acetyl (**1b**–**3b**) pyrazolines to 1J3I.pdb

Compounds	–CDOCKER (kcal/mol)	Interactions
1a	41.9928	H bonds: SER108
		π Bonds: ALA16, LEU46 (2 bonds), PHE58, ILE112, PRO113
2a	51.2603	H bonds: CYS 15, ASP 54 (3 bonds), SER 108
		π bonds: LEU 40, LEU 46, PHE 58, ILE 112, PRO 113
3a	56.3316	H bonds: GLY44, SER108, SER111 (2 bonds), PHE116, SER 120, ILE164
		π Bonds: ALA 16, LEU46, MET55, PHE58, ILE112, PHE116, LEU119
1b	48.8774	H bonds: SER 108, SER 111
		π bonds: ALA 16, VAL 45, LEU 46 (2 bonds), PHE 58, ILE 112, PRO 113
2b	45.5088	H bonds: ALA 16 (2 bonds), LEU40, SER108, SER 111
		π bonds: LEU 46 (3 bonds), ILE 112, PRO 113
3b	39.035	H bonds: ALA 16 (2 bonds), LEU 40, GLY 165
		π bonds: LEU 46, MET 55, PHE 58, ILE 112, PHE 116
WR99210	54.32	H bonds: ALA16, ILE164, PHE58, TYR170, SER108, ILE14, ASP54, CYS15
		π bonds: LEU164, MET55

The lowest docking energy was displayed by **3a**, **2a,** and **1b** with CDOCKER energies of –56.316, –51.2603, and –48.8774 kcal/mol, respectively. The lower CDOCKER energy is preferred for showing a more stable interaction between ligand and protein which could lead to better bioactivity of the molecules. Therefore, it can be noticed that the order of the CDOCKER energy was in accordance with the *in vitro* antimalarial test.

Table 2 implies that there is a correlation between the number of hydrogen bonds and the CDOCKER energy. An increasing number of hydrogen bonds to the amino acids of the receptor active site is expected to increase the binding efficiency (with lower docking energy) and also the inhibition (bioactivity) (Kumar et al. 2014). The hydrogen bonding is essential factor in the inhibition of complex molecules which provides the stability of structure and functions (Ibrahim et al. 2020). The N-phenyl pyrazoline **3a** has formed seven hydrogen bonds with GLY44, SER108, SER111, PHE116, SER120, and ILE164, as well as eight π-bonds to ALA16, LEU46, MET55, PHE58, ILE112, PHE116, and LEU119. Meanwhile, the other pyrazolines formed less hydrogen bonding to the respected amino acid residues so they had higher docking energies. Thus, pyrazoline **3a** was proposed as the best antimalarial activity followed by **2a** proved by the *in vitro* assay and Molecular docking studies.

This work also proposed the importance of some interactions to the essential amino acid residues. Compound **3a** possessed five similar interactions to the native co-crystal ligand WR99210, such as SER108, ILE164, ALA16, MET55, and PHE58. It can also be noted

that except **3a**, the other compounds formed fewer similar interactions to WR99210. The presence of interactions with those amino acid residues is essential to determine the stability of the complex, where the hydrogen bond is preferred (Yuvaniyama et al. 2003). The *in-silico* docking study also proposed the importance of hydrogen bonds to GLY44 (pyrazoline **3a**) in the interaction of the *Pf*DHFR-TS crystal protein (1j3I.pdb) (Hadni & Elhaloui 2019; Purwono et al. 2021; Septiana et al. 2022).

Visualization of the interaction in Table 3 indicates the importance of the methoxy group in the formation of hydrogen bonds. Only one methoxy group in N-phenyl

pyrazoline **2a** participates in the formation of hydrogen bonds, while three methoxy groups in N-phenyl pyrazoline **3a** are involved in the interactions. Meanwhile, only one methoxy group in N-acetyl pyrazoline **2b** and two methoxy groups in **3b** are responsible for the formation of hydrogen bonds. The pyrazoline ring is also responsible for the formation of π-bonds with the respected amino acid residues. The phenyl group that attached to the N atom of the pyrazoline ring also displayed interaction with essential amino acid residues. The acetyl group in pyrazolines **1b** and **2b** also participated in the formation of hydrogen bonds.

TABLE 3. 3D and 2D visualization of the interactions of N-phenyl (**1a–3a**) and N-acetyl (**1b–3b**) pyrazolines to 1J3I.pdb
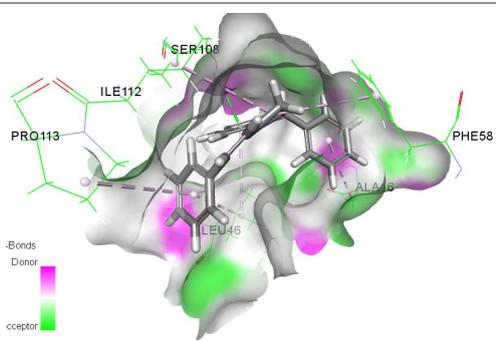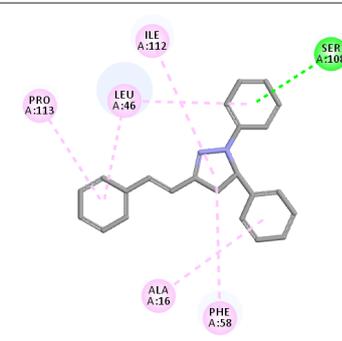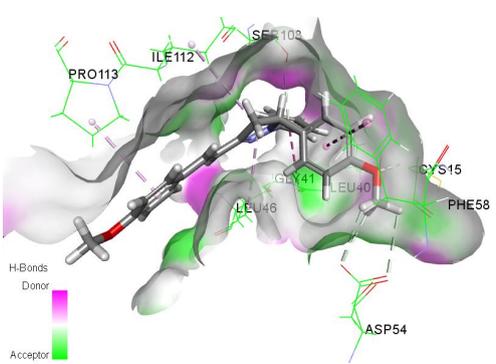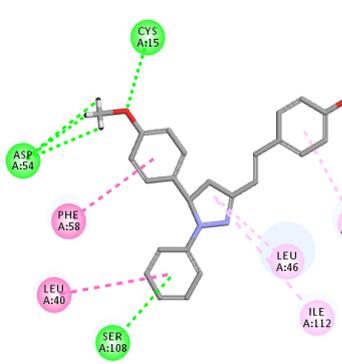
Code	3D	2D
1a		
2a		
3a		
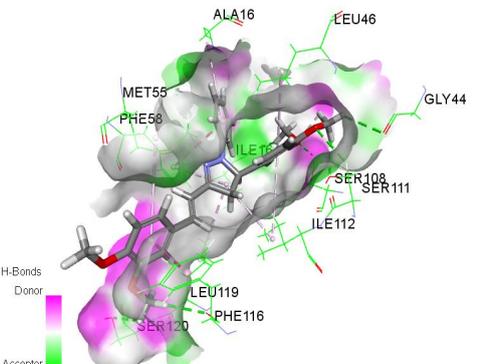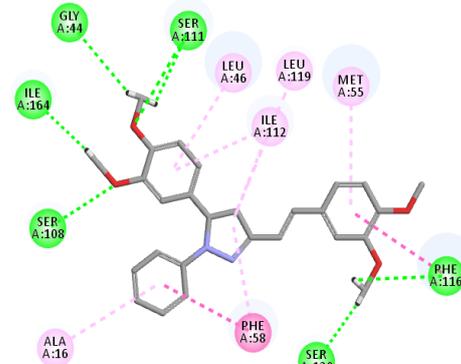
1b
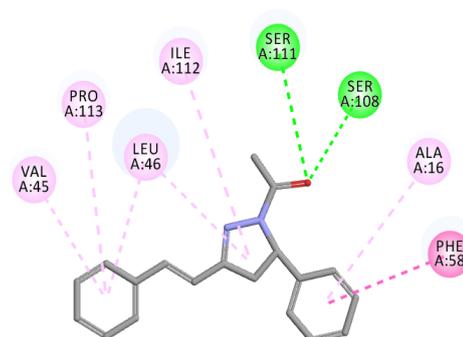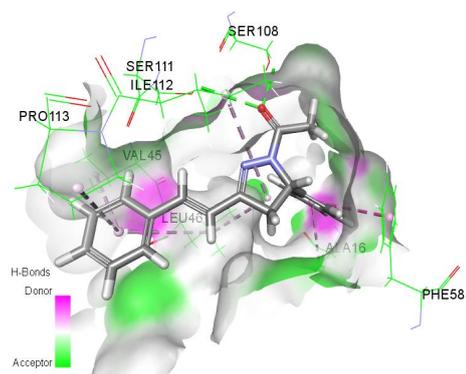
2b
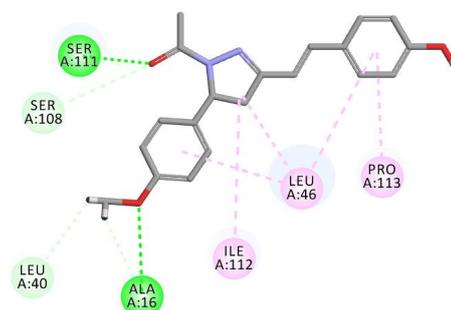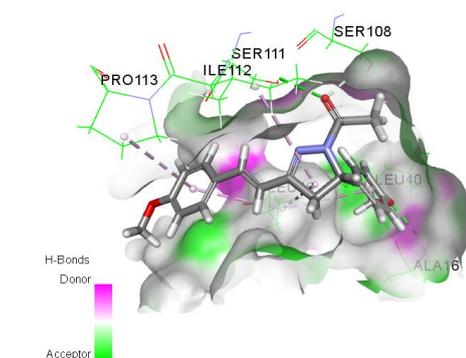
3b
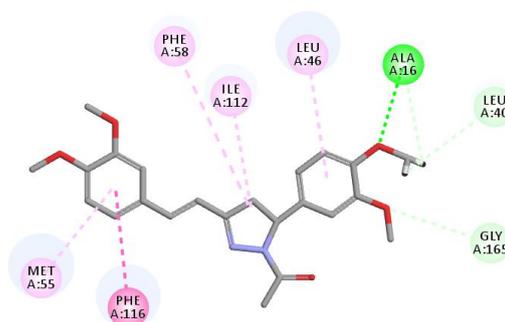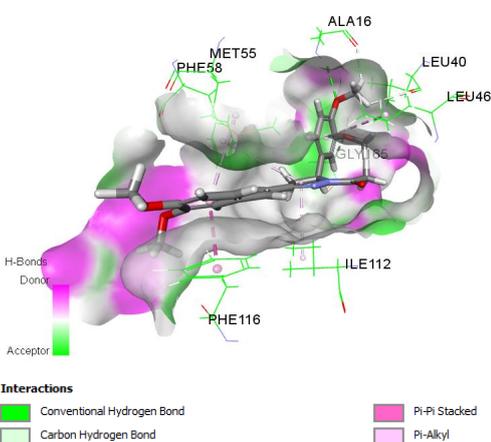
Interactions

■ Conventional Hydrogen Bond	■ Pi-Pi Stacked
■ Carbon Hydrogen Bond	■ Pi-Alkyl

DRUG-LIKENESS PREDICTION

It has been proposed that Lipinski's rules can be used as a guideline to predict the probability of a drug candidate being bioavailable when taken orally (by humans) (Tyagi et al. 2019). Therefore, by obeying this rule, a compound can be proposed to be orally bioavailable. This rule is related to the physicochemical properties of molecules, including hydrophobicity, hydrogen bonding, molecular weight, bioavailability, and toxicity (Ertl et al. 2000). Drug-like evaluation according to Lipinski's rule offers a prediction of the solubility and biological barrier-crossing factors such as absorption and brain access (Daina et al. 2017). The predicted physicochemical properties of the N-phenyl (**1a–3a**) and N-acetyl (**1b–3b**) pyrazolines are presented in Table 4.

TABLE 4. Prediction of druglikeness and ADMET parameters of N-phenyl (**1a**–**3a**) and N-acetyl (**1b**–**3b**) pyrazolines

Parameters	1a	2a	3a	1b	2b	3b
Drug-likeness						
• Molecular weight	324.160	384.180	444.200	290.140	350.160	410.180
• H-bond acceptor	2	4	6	3	5	7
• H-bond donor	0	0	0	0	0	0
• LogP	5.140	5.327	4.571	3.534	3.645	2.834
A (Absorption)						
• Human intestinal absorption (HIA)	− −	− − −	− − −	− − −	− − −	− − −
• Caco-2 permeability (log cm/s)	−4.886	−4.887	−4.992	−4.736	−4.717	−4.803
• P-glycoprotein inhibitor	− −	+++	+++	+++	+++	+++
• P-glycoprotein substrate	− − −	− − −	− −	− − −	− − −	− − −
• $F_{20\%}$	+++	− − −	− − −	− − −	− − −	− − −
• $F_{30\%}$	− − −	− − −	++	− − −	− − −	++
D (Distribution)						
• Plasma protein binding (PPB) (%)	97.760	98.359	97.400	95.100	95.970	95.088
• Blood-brain barrier penetration (BBB) (cm/s)	++	−	− −	+++	+++	+++
• Volume distribution (L/kg)	0.727	0.779	0.454	0.862	0.932	0.721
M (Metabolism)						
• CYP1A2 substrate	− −	+++	+++	−	++	+++
• CYP1A2 inhibitor	+++	−	− −	+++	+	− − −
• CYP2C19 substrate	− − −	++	+++	++	+++	+++
• CYP2C19 inhibitor	+++	++	+++	+++	+++	+
• CYP2C9 substrate	+++	+++	++	++	++	+
• CYP2C9 inhibitor	+++	++	++	++	++	− −
• CYP2D6 substrate	−	+++	+++	− −	++	+
• CYP2D6 inhibitor	−	− − −	− − −	− − −	− − −	− − −
• CYP3A4 substrate	++	+++	+++	++	+++	+++
• CYP3A4 inhibitor	+	++	++	− −	++	+
E (Excretion)*						
• Half-life time ($T_{1/2}$)	0.184	0.127	0.732	0.606	0.358	0.840
• Clearance (mL/min/kg)	3.432	5.664	9.075	2.751	5.975	8.784
T (Toxicity)						
• Human hepatotoxicity	− − −	− −	− −	++	+++	++
• hERG blockers	− − −	−	− −	− − −	−	−
• Rat oral acute toxicity	− − −	− − −	− − −	− − −	− −	− −
• Ames toxicity	++	+++	++	+++	+++	++
• Drug-induced liver injury	+++	++	+++	++	++	++
• Carcinogenicity	++	++	+	+	++	++

Note: The different symbols represent prediction probability values: 0-0.1(− − −), 0.1-0.3(− −), 0.3-0.5(−), 0.5-0.7(+), 0.7-0.9(++), and 0.9-1.0(+++)

All of the prepared pyrazolines have a molecular weight of less than 450 and they were expected to have better brain permeation and good oral absorption (Pajouhesh & Lenz 2005). All of the synthesized pyrazolines do not possess a hydrogen bond donor (HBD). This result is favorable as a higher number of hydrogen bond acceptors is expected could lead to poor permeability across a membrane bilayer (Zerroug et al. 2019). N-phenyl (**1a–3a**) and N-acetyl (**1b–3b**) pyrazolines appeared to have two to seven hydrogen bond acceptors (HBA), which is in the optimal range in Lipinski's rules. Increasing the number of methoxy groups likely would increase the number of HBA due to the presence of the oxygen atom.

LogP plays an important factor in the lipophilicity, ADME properties, and pharmacological activity (Zorroug et al. 2019). Lipinski's rules require that a compound have a partition coefficient (logP) value of <5, while good oral bioavailability (good permeability and solubility) can be achieved if the molecules have a moderate logP ($0 < \log P < 3$). This rule comes from understanding that a high logP means drug possessing low aqueous solubility, poor oral absorption, and an increased risk of toxicity. On the contrary, a very low logP makes the drug difficult to penetrate the lipid bilayer of cell membranes and might affect its efficacy. According to this rule, only pyrazoline **1a** and **2a** have logP values > 5, indicating the higher lipophilic properties of these two compounds. Pyrazolines **3a**, **1b**, and **2b** have a logP value in the range of 3-5, while **3b** is the only compound that has a logP < 3. These values indicated that the phenyl group tend to increase the lipophilic properties of molecules.

Based on this work, N-phenyl pyrazolines **1a** and **2a** violated one rule which their logP values were above the normal range. However, a compound is only considered to be orally not bioavailable if it violates two or more parameters of Lipinski's rule (Ibrahim et al. 2020). Therefore, the N-phenyl (**1a–3a**) and N-acetyl (**1b–3b**) pyrazoline compounds could be proposed as drug candidates based on the oral bioavailability parameters by Lipinski's rule of five.

PREDICTION OF ADMET PARAMETERS

A molecule can be defined as an effective drug if it can reach the target in the body in an adequate concentration and remain in a bioactive form long enough for the expected biological activity to happen (Daina et al. 2017). Therefore, pharmacokinetic assessment is important as part of the drug discovery and development involving the evaluation of some pharmacological parameters, such as absorption, distribution, metabolism, excretion (ADME), and toxicological (T) aspects. In this work, prediction of ADMET parameters of N-phenyl (**1a–3a**) and N-acetyl (**1b–3b**) pyrazolines was performed *in silico* from the molecular structure in an attempt to propose the best antimalarial drug candidates (Table 4).

The absorption profile of the N-phenyl (**1a–3a**) and N-acetyl (**1b–3b**) pyrazolines by the HIA parameter was shown to be negative. This result means that the prepared compounds were predicted to have an intestinal absorbance >30%. Additionally, all of the N-phenyl (**1a–3a**) and N-acetyl (**1b–3b**) were predicted to have good membrane permeability as shown by Caco-2 permeability log values that are higher than –5.15. Table 4 also shows that only pyrazoline **1a** behaved as a non-inhibitor of P-glycoprotein, while all of the pyrazolines were non-substrates of P-glycoprotein (negative). Based on the human oral bioavailability ($F_{20\%}$ and $F_{30\%}$) indicators, only pyrazoline **1a** was predicted to have a bioavailability <20%, whereas pyrazoline **3a** and **3b** had a bioavailability ≥30%.

All the N-phenyl (**1a–3a**) and N-acetyl (**1b–3b**) pyrazolines were predicted to have poor PPB as they have output values higher than 90%, indicating a high plasma protein-bound and low therapeutic index. On the other hand, pyrazoline **3a** was expected to possess the lowest BBB penetration (–), whereas **2a** has a higher chance of crossing the BBB (– –). The distribution volume (VD) describes the *in vivo* distribution of drugs, such as binding to plasma protein, the distribution amount in body fluid, and the uptake amount in tissues. According to our studies, all of the prepared compounds were predicted to have proper VD values in the range of 0.04–20 L/kg. However, it could be pointed out that pyrazoline **3a** is considered to have a relatively low distribution volume as its VD value is lower than 0.7 L/kg (Han et al. 2019). In terms of metabolism, N-phenyl (**1a–3a**) and N-acetyl (**1b–3b**) pyrazolines were evaluated toward Cytochrome P450 (CYP), which is an important enzyme in the metabolism of drugs. The induction and inhibition of CYPs are essential mechanisms leading to pharmacokinetic drug-drug interactions (Hakkola et al. 2020). Table 4 displays the prediction of pyrazolines as inhibitors or substrates for CYP1A2, CYP2C19, CYP2C9, CYP2D6, and CYP3A4 isozymes. Compound **1a** was predicted to be CYP2C9 and CYP3A4 substrates as well as a non-inhibitor of CYP2D6. Both pyrazoline **2a** and **3a** acted as substrates for all of the isozymes but were non-inhibitors to CYP1A2 and CYP2D6. N-acetyl pyrazoline **1b** was considered to be a non-substrate for CYP1A2

and CYP2D6. From Table 4, it can also be predicted that **1b** might be non-inhibitors for CYP2D6 and CYP3A4. Compound **2b** was proposed to act as a substrate for all of the isozymes and only be a strong non-inhibitor for CYP2D6. Meanwhile, pyrazoline **3b** acted as a substrate for all isozymes and did not inhibit CYP1A2, CYP2C9, and CYP2D6.

The excretion of the compounds was assessed by the half-life (t½) and clearance parameters. Table 4 shows that pyrazolines **1a** and **2a** have t½ probability values of < 0.2 (excellent), indicating that both compounds have a half-life of < 3 hours (short half-life). On the other hand, **3a** and **3b** were shown to have t½ probability values of > 0.7 (poor), suggesting the half-life for both compounds were longer than pyrazolines **1a** and **2a**. The clearance rate of compounds **1a** and **2a** was categorized as low clearance (<5 mL/min/kg), decided as a poor result. Furthermore, the other compounds were predicted to have moderate clearance (5-15 mL/min/kg) with the highest clearance rate by **3a**.

Toxicity evaluation is important to ensure the safety of drugs with no harm or any kind of side effect. The human hepatotoxicity assessment shows that N-phenyl (**1a**–**3a**) pyrazolines were classified as negative, indicating an excellent result. On the contrary, the N-acetyl (**1b**–**3b**) pyrazolines were predicted to be hepatotoxic (positive). All of the prepared pyrazolines showed a good outcome as non-hERG blockers (negative) and may have low rat oral acute toxicity (negative). The results in Table 4 also indicate that all of the prepared pyrazolines were at a high risk of inducing a liver injury (positive), being carcinogenic (positive), and may be toxic in the Ames test (positive). Based on this result, all of the prepared pyrazoline compounds were predicted to be relatively toxic with at least one positive result in the toxicity parameters (Dong et al. 2018). The toxicity of molecules is related to their lipophilicity. As the lipophilicity increases, there is more potential for being toxic because of an increased probability of binding to hydrophobic protein targets other than the desired one (Pajouhesh & Lenz 2005). Thus, it is proposed further modifications to reduce toxicity and lipophilicity.

CONCLUSIONS

Based on our studies of *in vitro* assay against the *P. falciparum* 3D7 strain, molecular docking against *Pf*DHFR-TS (PDB ID: 1J3I and drug-likeness prediction, pyrazolines **3a**, **2a**, and **1b** are potential to be developed as antimalarial lead compounds and predicted to be orally bioavailable according to Lipinski's rules. The ADMET

analysis points out that the compounds may be toxic. Hence, further structural modifications are suggested to decrease toxicity and lipophilicity.

REFERENCES

Adebayo, J.O., Tijjani, H., Adegunloye, A.P., Ishola, A.A., Balogun, E.A. & Malomo, S.O. 2020. Enhancing the antimalarial activity of artesunate. *Parasitology Research* 119(9): 2749-2764.

Aher, R.B., Wanare, G., Kawathekar, N., Kumar, R.R., Kaushik, N.K., Sahal, D. & Chauhan, V.S. 2011. Dibenzylideneacetone analogues as novel *Plasmodium falciparum* inhibitors. *Bioorganic and Medicinal Chemistry Letters* 21(10): 3034-2036.

Batista, R., Silva, A.J. Jr. & de Oliveira, A.B. 2009. Plant-derived antimalarial agents: New leads and efficient phytomedicines. Part II. Non-alkaloidal natural products. *Molecules* 14(8): 3037-3072.

Belete, T.M. 2020. Recent progress in the development of new antimalarial drugs with novel targets. *Drug Design, Development and Therapy* 14: 3875-3889.

Charris, J.E., Monasterios, M.C., Acosta, M.E., Rodríguez, M.A., Gamboa, N.D., Martínez, G.P., Rojas, H.R., Mijares, M.R. & De Sanctis, J.B. 2019. Antimalarial, antiproliferative, and apoptotic activity of quinoline-chalcone and quinoline-pyrazoline hybrids. A dual action. *Medicinal Chemistry Research* 28: 2050-2066.

Chugh, A., Kumar, A., Verma, A., Kumar, S. & Kumar, P. 2020. A review of antimalarial activity of two or three nitrogen atoms containing heterocyclic compounds. *Medicinal Chemistry Research* 29: 1723-1750.

Daina, A., Michielin, O. & Zoete, V. 2017. SwissADME: A free web tool to evaluate pharmacokinetics, drug-likeness and medicinal chemistry friendliness of small molecules. *Scientific Report* 7: 42717.

de Souza, J.E., do Nascimento, M.F.A., Borsodi, M.P.G., de Almeida, A.P., Rossi-Bergmann, B., de Oliveira, A.B. & Costa, S.S. 2018. Leaves from the tree *Poincianella pluviosa* as a renewable source of antiplasmodial compounds against chloroquine-resistant *Plasmodium falciparum*. *Journal of the Brazilian Chemical Society* 29(6): 1318-1327.

Dong, J., Wang, N.N., Yao, Z.J., Zhang, L., Cheng, Y., Ouyang, D., Lu, A.P. & Cao, D.S. 2018. ADMETlab: A platform for systematic ADMET evaluation based on a comprehensively collected ADMET database. *Journal of Cheminformatics* 10(1): 29.

Ekawati, L., Purwono, B. & Mardjan, M.I.D. 2020. Synthesis N-phenyl pyrazoline from dibenzalacetone and heme polymerization inhibitory activity (HPIA) assay. *Key Engineering Materials* 840: 245-250.

Ertl, P., Rohde, B. & Selzer, P. 2000. Fast calculation of molecular polar surface area as a sum of fragment-based contributions and its application to the prediction of drug transport properties. *Journal of Medicinal Chemistry* 43(20): 3714-3717.

Hadni, H. & Elhallaoui, M. 2019. Molecular docking and QSAR studies for modeling the antimalarial activity of hybrids 4-anilinoquinoline-triazines derivatives with the wild-type and mutant receptor *pf*-DHFR. *Heliyon* 5(8): e02357.

Han, Y., Zhang, J., Hu, C.Q., Zhang, X., Ma, B. & Zhang, P. 2019. *In silico* ADME and toxicity prediction of ceftazidime and its impurities. *Frontiers in Pharmacology* 10: 434.

Hakkola, J., Hukkanen, J., Turpeinen, M. & Pelkonen, O. 2020. Inhibition and induction of CYP enzymes in humans: An update. *Archives of Toxicology* 94: 3671-3722.

Ibrahim, Z.Y., Uzairu, A., Shallangwa, G. & Abechi, S. 2020. Molecular docking studies, drug-likeness and *in-silico* ADMET prediction of some novel β-Amino alcohol grafted 1,4,5-trisubstituted 1,2,3-triazoles derivatives as elevators of p53 protein levels. *Scientific African* 10: e00570.

Kalaria, P.N., Karad, S.C. & Raval, D.K. 2018. A review on diverse heterocyclic compounds as the privileged scaffolds in antimalarial drug discovery. *European Journal of Medicinal Chemistry* 158: 917-936.

Kumar, P., Choonara, Y.E. & Pillay, V. 2014. *In silico* affinity profiling of neuroactive polyphenols for post-traumatic calpain inactivation: A molecular docking and atomistic simulation sensitivity analysis. *Molecules* 20(1): 135-168.

Leroy, D. 2017. How to tackle antimalarial resistance? *EMBO Molecular Medicine* 9(2): 133-134.

Lipinski, C.A., Lombardo, F., Dominy, B.W. & Feeney, P.J. 2001. Experimental and computational approaches to estimate solubility and permeability in drug discovery and development settings. *Advanced Drug Delivery Review* 46(1-3): 3-26.

Manohar, S., Khan, A.I., Kandi, A.K., Raj, K., Sun, G., Yang, X., Molina, A.D.C., Wang, B. & Rawat, D.S. 2013. Synthesis, antimalarial activity and cytotoxic potential of new monocarbonyl analogues of curcumin. *Bioorganic and Medicinal Chemistry Letters* 23(1): 112-116.

Nauduri, D. & Reddy, G.B.S. 1998 Antibacterial and antimycotics Part 1: Synthesis and activity of 2-Pyrazolines derivatives. *Chemical and Pharmaceutical Bulletin* 46(8): 1254-1260.

Nigam, M., Atanassova, M., Mishra, A.P., Pezzani, R., Devkota, H.P., Plygun, S., Salehi, B., Setzer, W.N. & Sharifi-Rad, J. 2019. Bioactive compounds and health benefits of Artemisia species. *Natural Product Communications* 14(7): 1-17.

Pajouhesh, H. & Lenz, G.R. 2005. Medicinal chemical properties of successful central nervous system drugs. *NeuroRx* 2(4): 541-553.

Pandey, A.K., Sharma, S., Pandey, M., Alam, M.M., Shaquiquzzaman, M. & Akhter, M. 2016. 4,5-Dihydrooxazole-pyrazoline hybrids: Synthesis and their evaluation as potential antimalarial agents. *European Journal of Medicinal Chemistry* 123: 476-486.

Purwono, B., Nurohmah, B.A., Fathurrohman, P.Z. & Syahri, J. 2021. Some 2-arylbenzimidazole derivatives as an antimalarial agent: Synthesis, activity assay, molecular docking and pharmacological evaluation. *Rasayan Journal of Chemistry* 14(1): 94-100.

Septiana, I., Purwono, B., Anwar, C., Nurohmah, B.A. & Syahri, J. 2022. Synthesis and docking study of 2–Aryl-4,5-diphenyl-1H-imidazole derivatives as lead compounds for antimalarial agent. *Indonesian Journal of Chemistry* 22(05). https://doi.org/10.22146/ijc.67777

Sharma, N., Mohanakrishnan, D. & Shard, A. 2012. Stilbene-chalcone hybrids: Design, synthesis, and evaluation as a new class of antimalarial scaffolds that trigger cell death through stage specific Apoptosis. *Journal of Medicinal Chemistry* 55(1): 297-311.

Syahri, J., Nasution, H., Nurohmah, B.A., Purwono, B. & Yuanita, E. 2020a. Novel aminoalkylated chalcone: Synthesis, biological evaluation, and docking simulation as potent antimalarial agents. *Journal of Applied Pharmaceutical Science* 10(6): 1-005.

Syahri, J., Nasution, H., Nurohmah, B.A., Purwono, B., Yuanita, E. & Hassan, N.I. 2020b. Design, synthesis and biological evaluation of aminoalkylated chalcones as antimalarial agent. *Sains Malaysiana* 49(11): 2667-2677.

Tse, E.G., Korsik, M. & Todd, M.H. 2019. The past, present and future of anti-malarial medicines. *Malaria Journal* 18(1): 93.

Tyagi, R., Rosa, B.A. & Mitreva, M. 2019. Chapter 12 - Omics-driven knowledge-based discovery of anthelmintic targets and drugs. In *In Silico Drug Design: Repurposing Techniques and Methodologies,* edited by Kunal Roy. Academic Press. pp. 329-358.

Wang, Y., Huang, W., Chen, S., Chen, S.Q. & Wang, S.F. 2011. Synthesis, structure and tyrosinase inhibition of natural phenols derivatives. *Journal of Chinese Pharmaceutical Science* 20: 235-244.

Wanare, G., Aher, R., Kawathekar, N., Ranian, R., Kaushik, N.K. & Sahal, D. 2010. Synthesis of novel -pyranochalcones and pyrazoline derivatives as *Plasmodium falciparum* growth inhibitor. *Bioorganic and Medicinal Chemistry Letters* 20(15): 4675-48678.

World Health Organization (WHO). 2020. *World Malaria Report 2020: 20 Years of Global Progress and Challenges*. Geneva. License: CC BY-NC-SA 3.0 IGO.

Xiong, G., Wu, Z., Yi, J., Fu, L., Yang, Z., Hsieh, C., Yin, M., Zeng, X., Wu, C., Lu, A., Chen, X., Hou, T. & Cao, D. 2021. ADMETlab 2.0: An integrated online platform for accurate and comprehensive predictions of ADMET properties. *Nucleic Acids Research* 49(W1): W5-W14.

Yuvaniyama, J., Chitnumsub, P., Kamchonwongpaisan, S., Vanichtanankul, J., Sirawaraporn, W., Taylor, P., Taylor, P., Walkinshaw, M.D. & Yuthavong, Y. 2003. Insights into antifolate resistance from malarial DHFR-TS structures. *Nature Structural & Molecular Biology* 10(5): 357-365.

Zerroug, A., Belaidi, S., BenBrahim, I., Sinha, L. & Chtita, S. 2019. Virtual screening in drug-likeness and structure/ activity relationship of pyridazine derivatives as anti-Alzheimer drugs. *Journal of King Saud University-Science* 31(4): 595-601.

*Corresponding author; email: purwono.bambang@ugm.ac.id
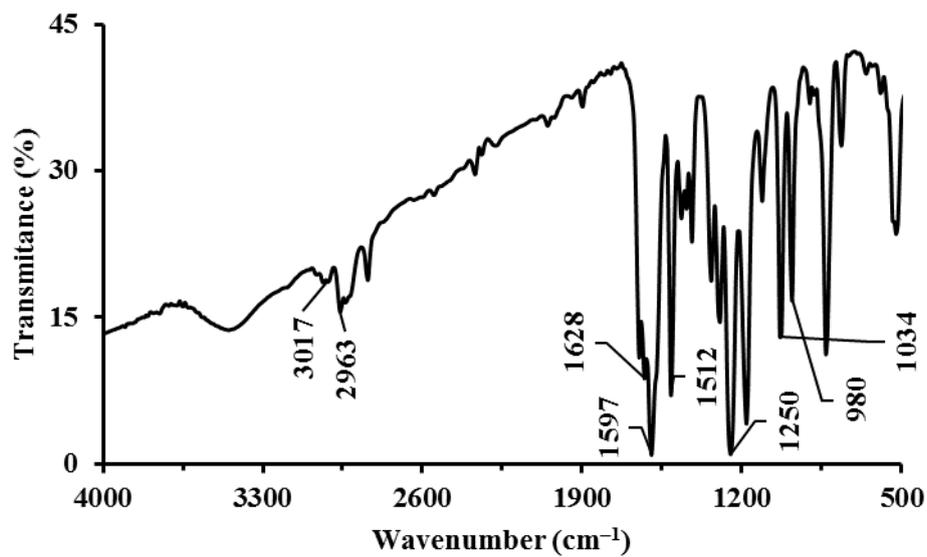
FIGURE S1. FTIR spectra of dibenzalacetone **2**
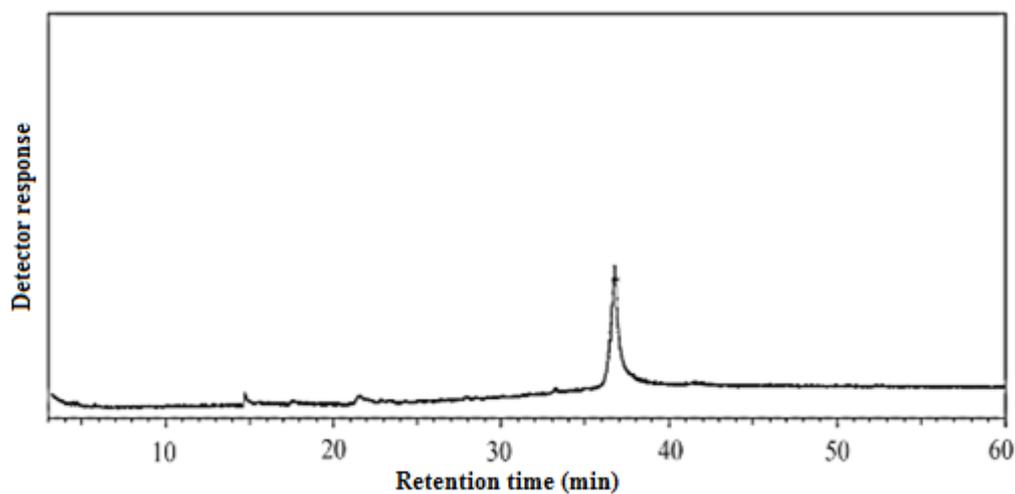
FIGURE S2. Gas chromatography (GC) spectra of dibenzalacetone **2**
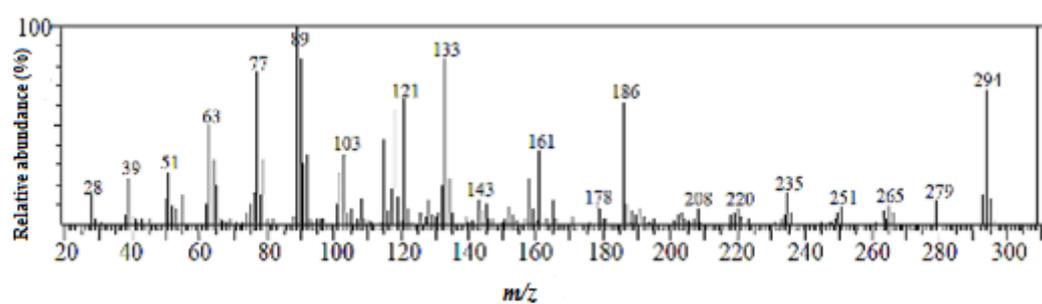
FIGURE S3. Mass spectra (MS) of dibenzalacetone **2**
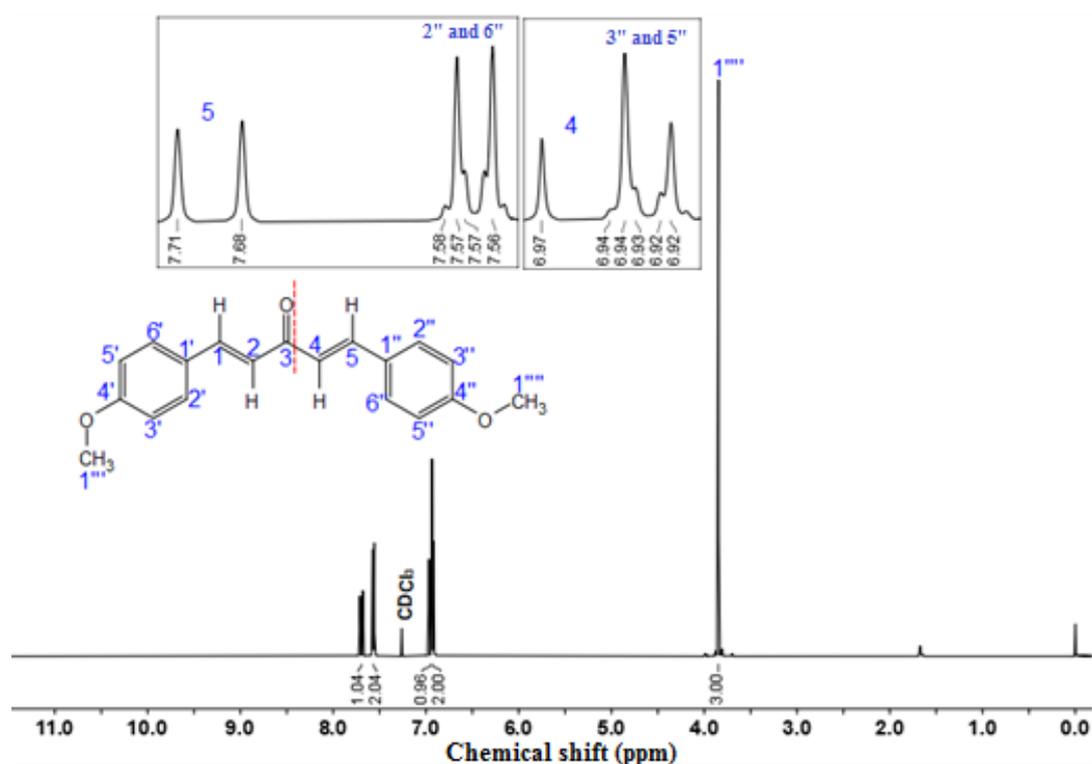
FIGURE S4. ¹H-NMR spectra of dibenzalacetone **2**
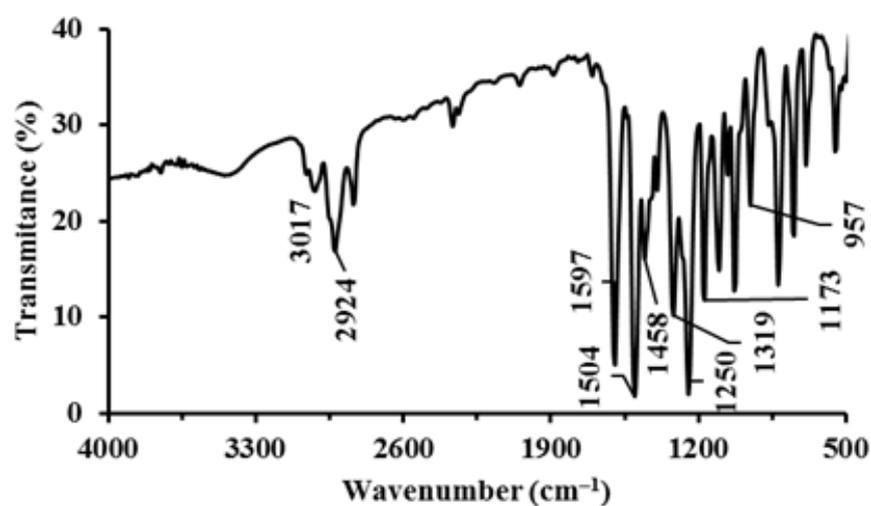
FIGURE S5. FTIR spectra of N-phenyl pyrazoline **2a**
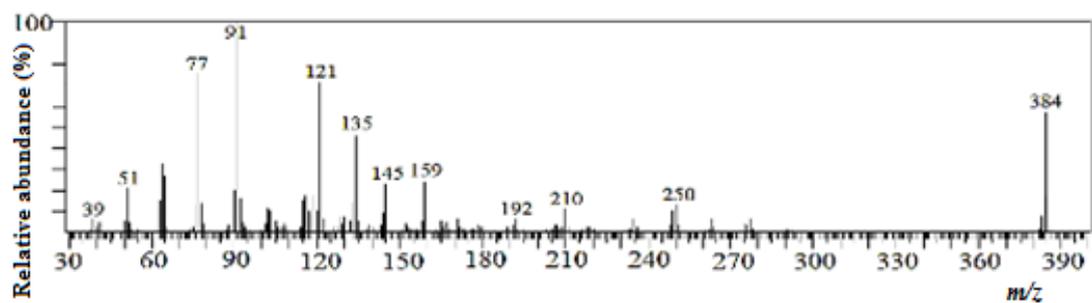
FIGURE S6. Mass spectra (MS) of N-phenyl pyrazoline **2a**
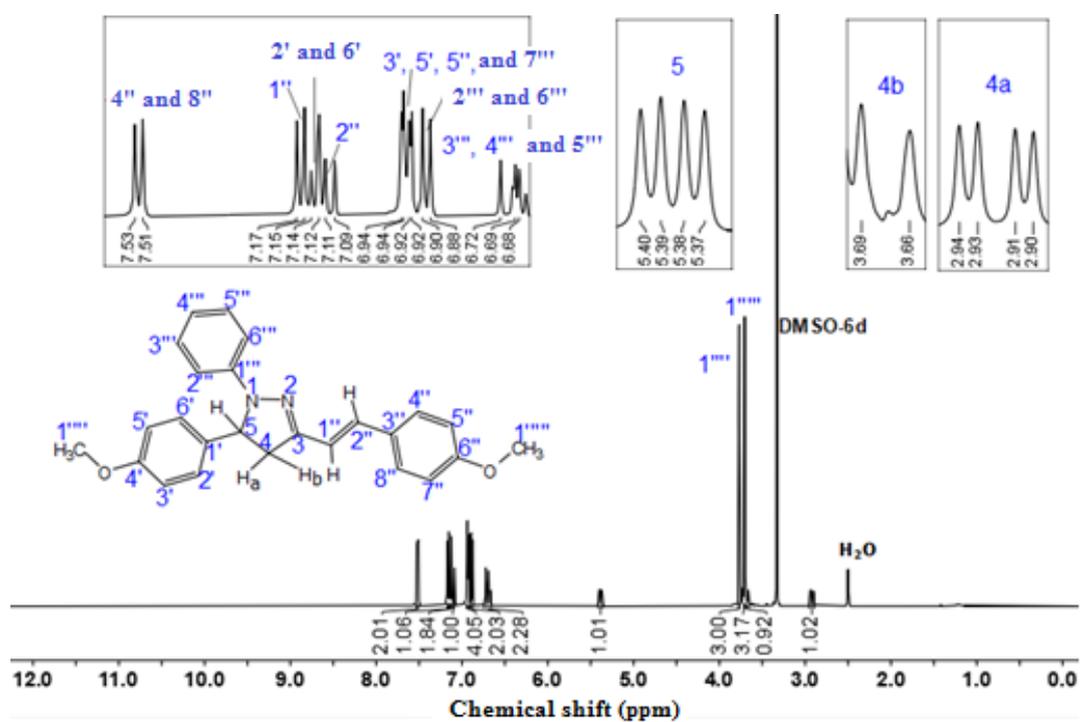
FIGURE S7. ¹H-NMR spectra of N-phenyl pyrazoline **2a**
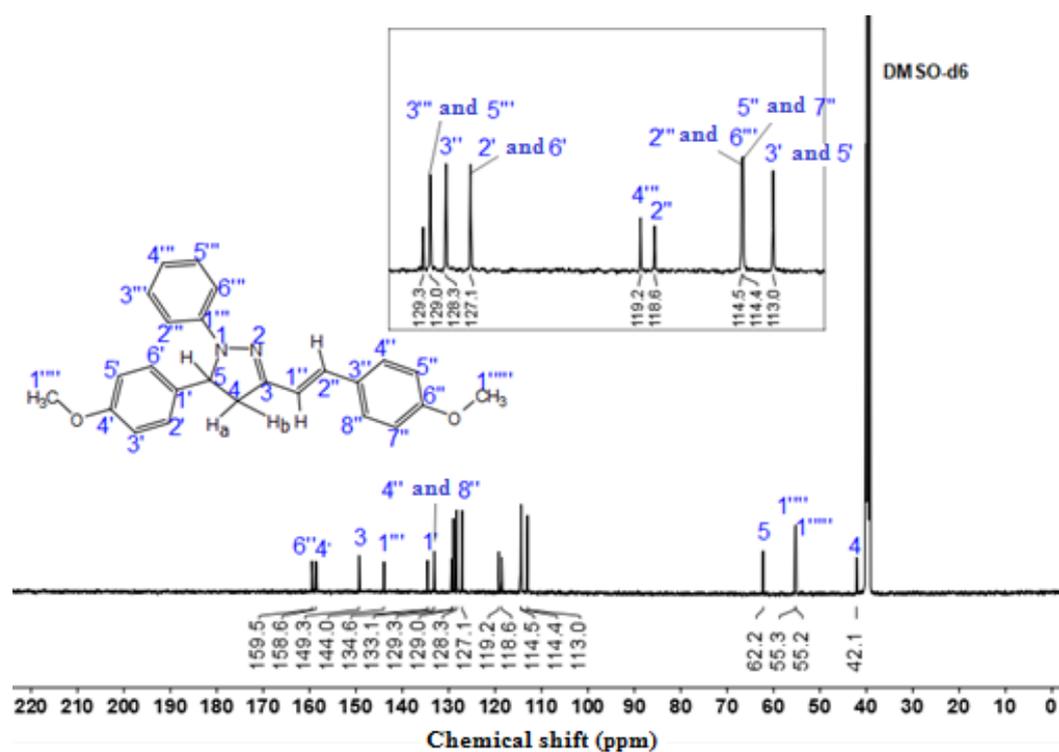
FIGURE S8. ^{13}C-NMR of N-phenyl pyrazoline **2a**
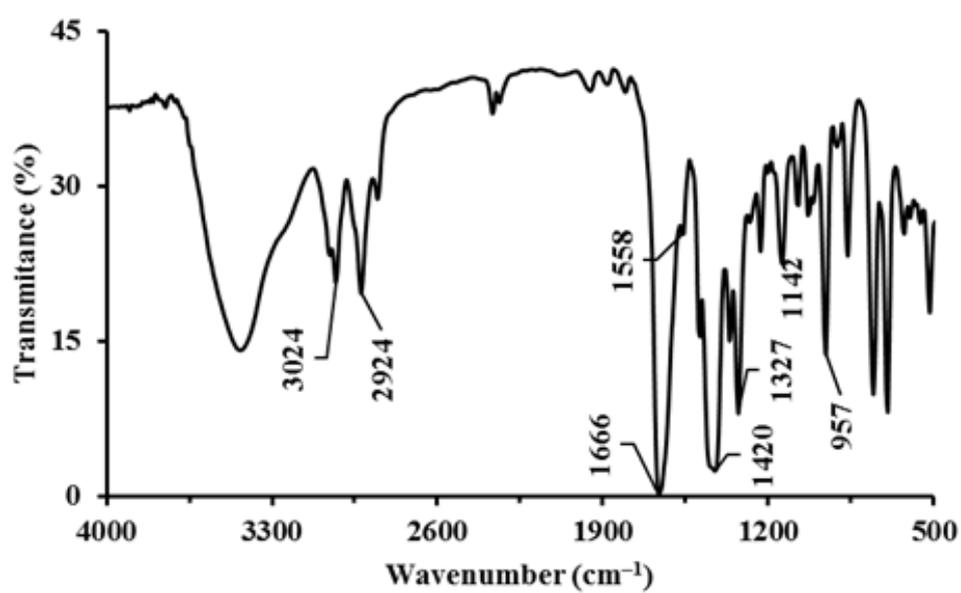
FIGURE S9. FTIR spectra of N-acetyl pyrazoline **1b**
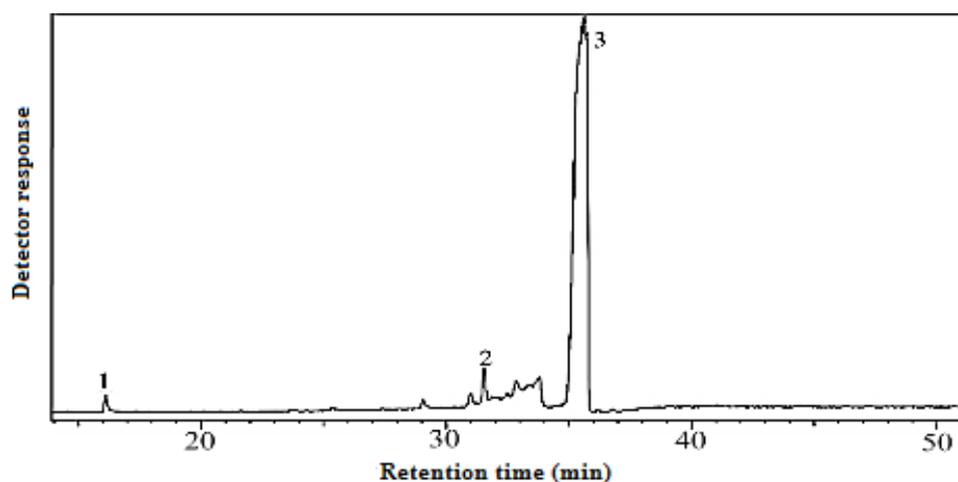
FIGURE S10. Gas chromatography (GC) spectra of N-acetyl pyrazoline **1b**
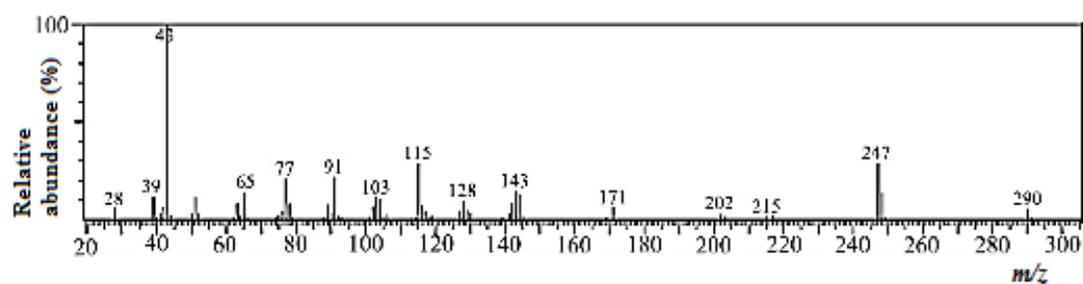
FIGURE S11. Mass spectra (MS) of N-acetyl pyrazoline **1b**
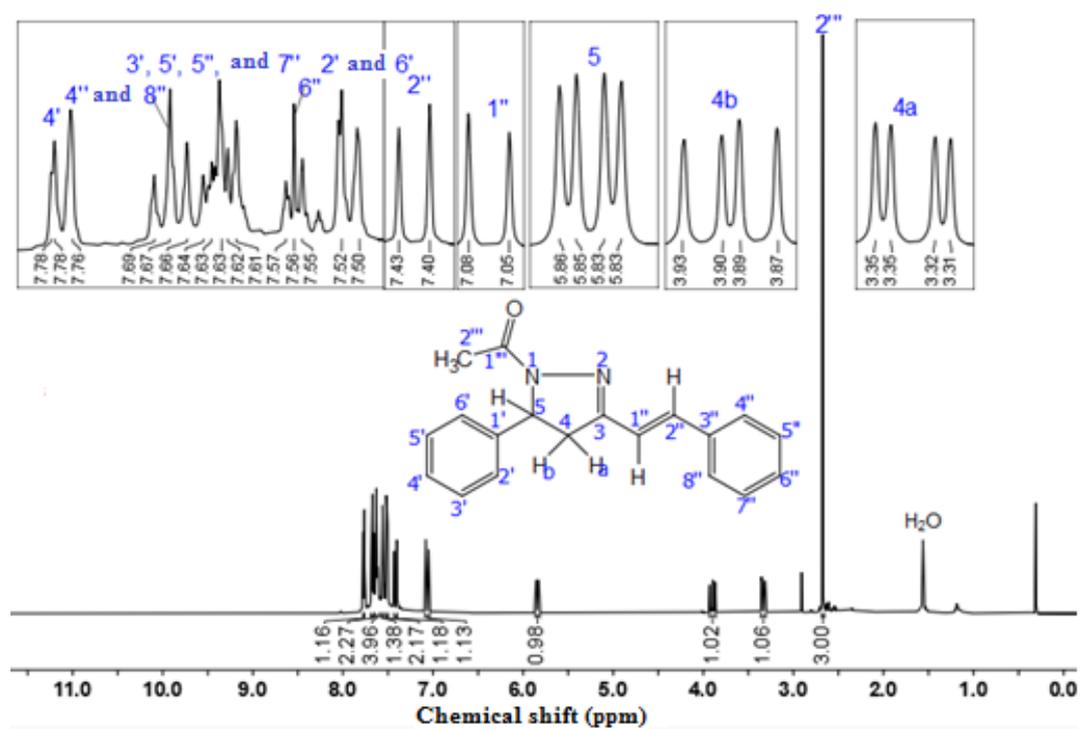
FIGURE S12. ^{1}H-NMR spectra of N-acetyl pyrazoline **1b**
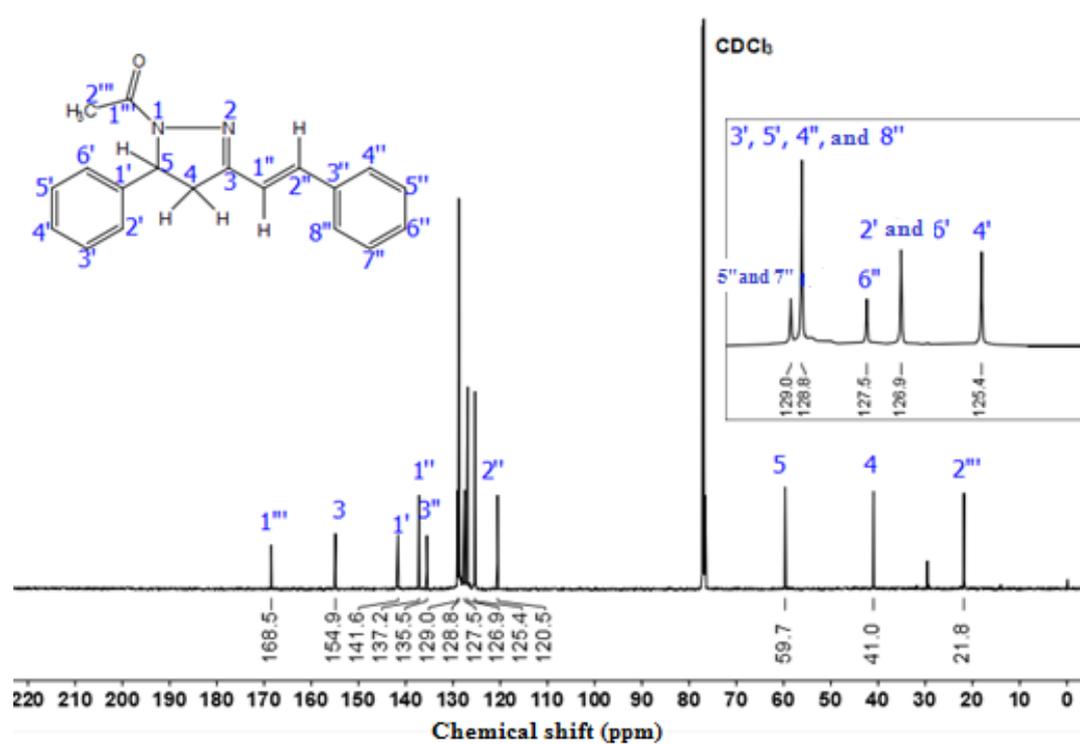
FIGURE S13. ^{13}C-NMR spectra of N-acetyl pyrazoline **1b**
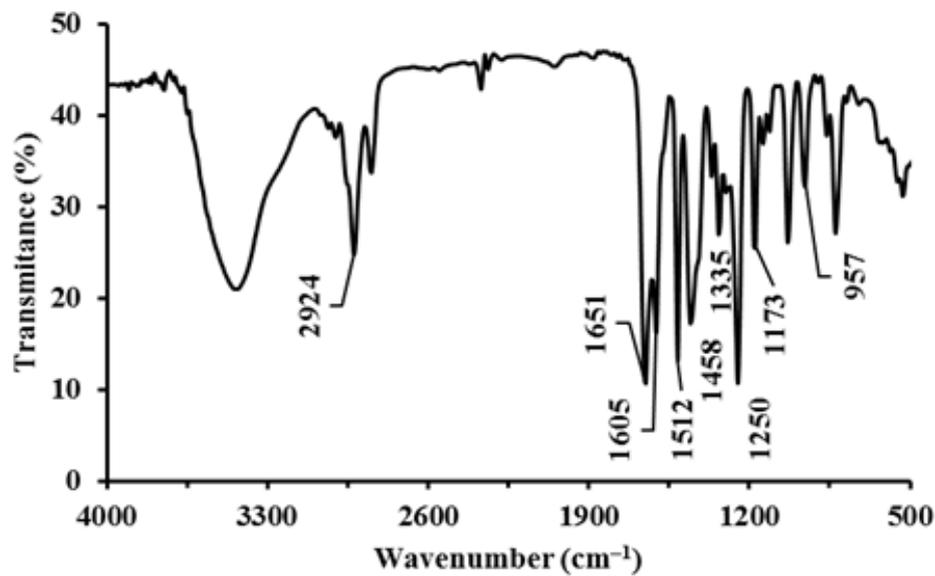
FIGURE S14. FTIR spectra of N-acetyl pyrazoline **2b**
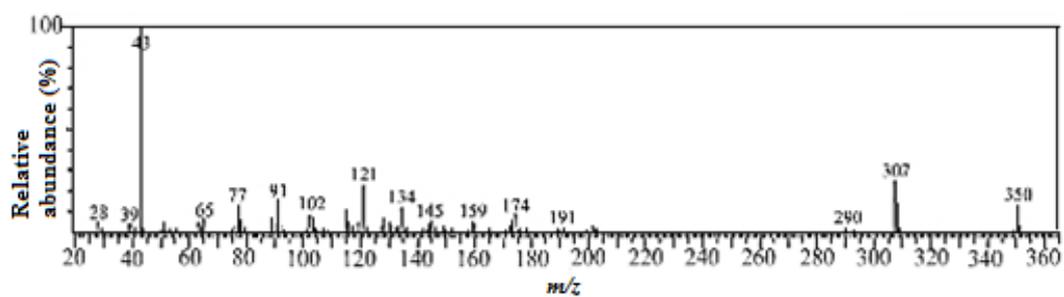
FIGURE S15. Mass spectra (MS) of N-acetyl pyrazoline **2b**
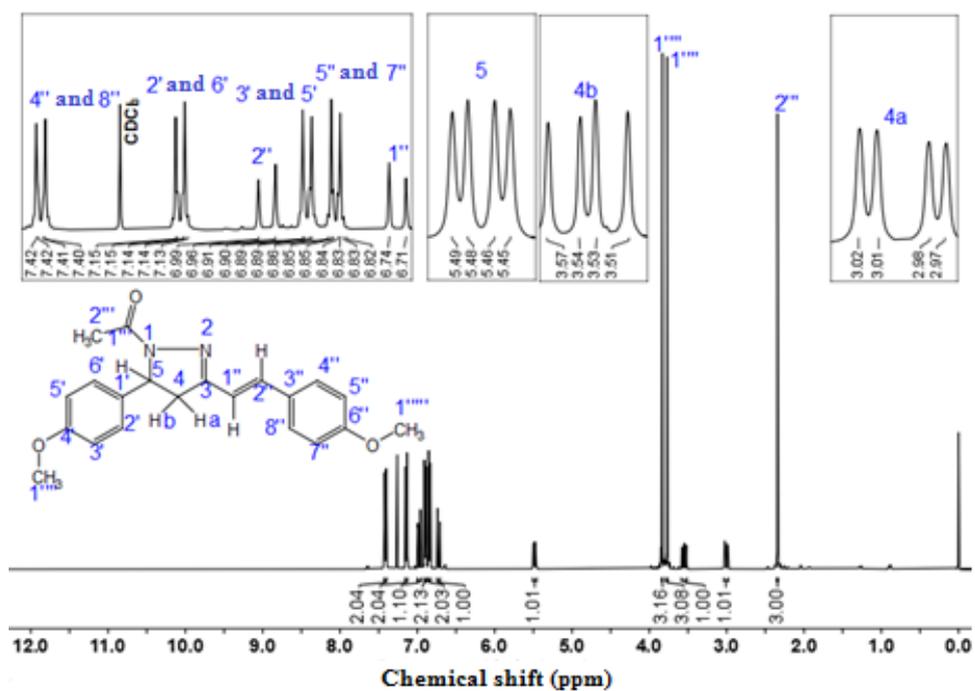
FIGURE S16. ¹H-NMR spectra of N-acetyl pyrazoline **2b**
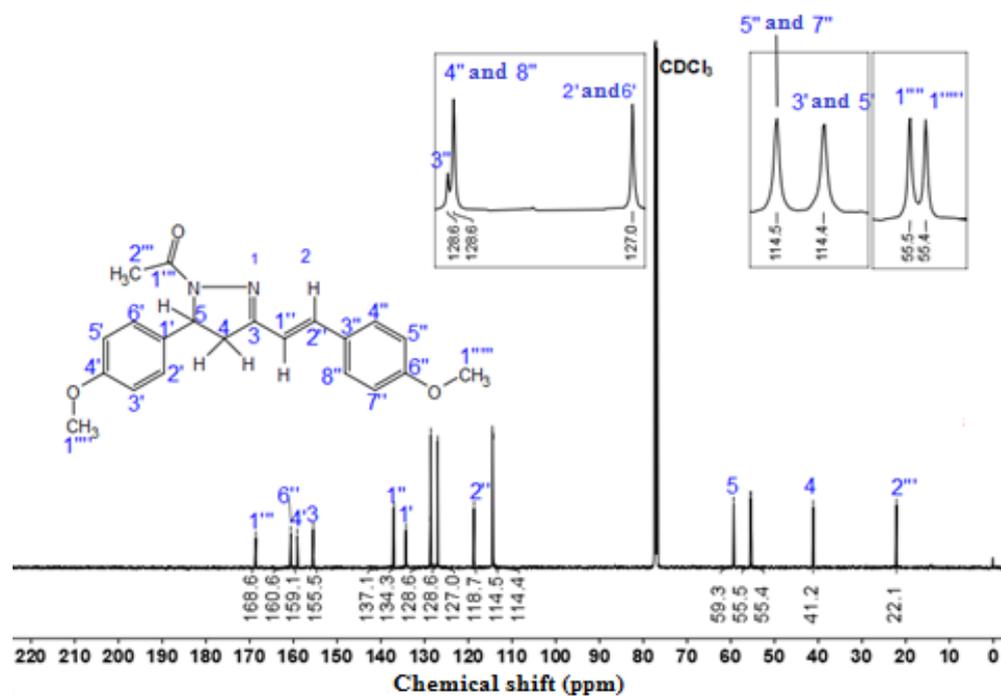
FIGURE S17. ¹³C-NMR spectra of N-acetyl pyrazoline **2b**
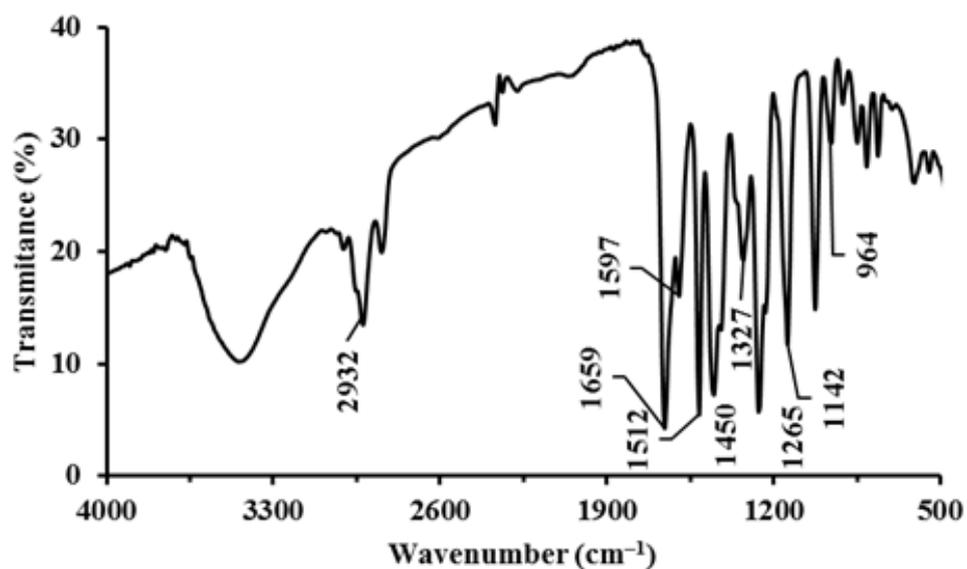
FIGURE S18. FTIR spectra of N-acetyl pyrazoline **3b**
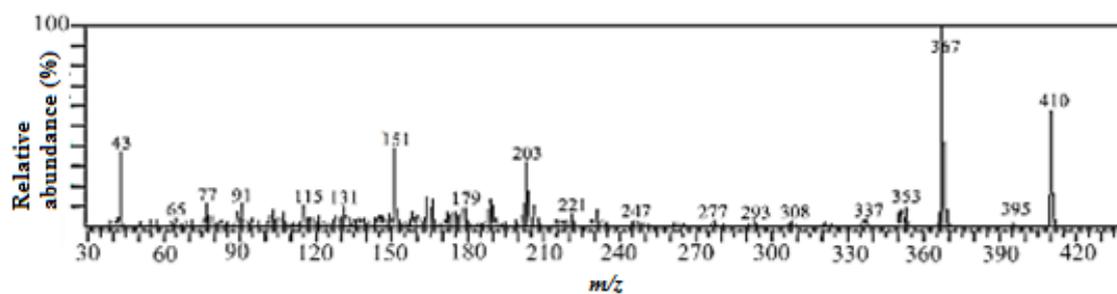
FIGURE S19. Mass spectra (MS) of N-acetyl pyrazoline **3b**
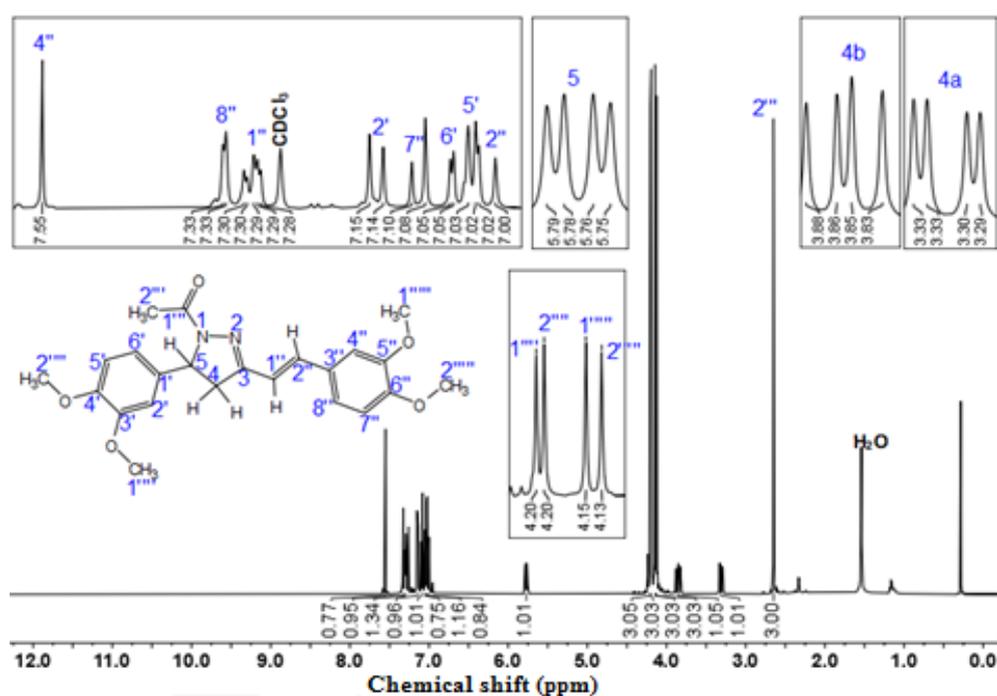
FIGURE S20. ^{1}H-NMR spectra of N-acetyl pyrazoline **3b**
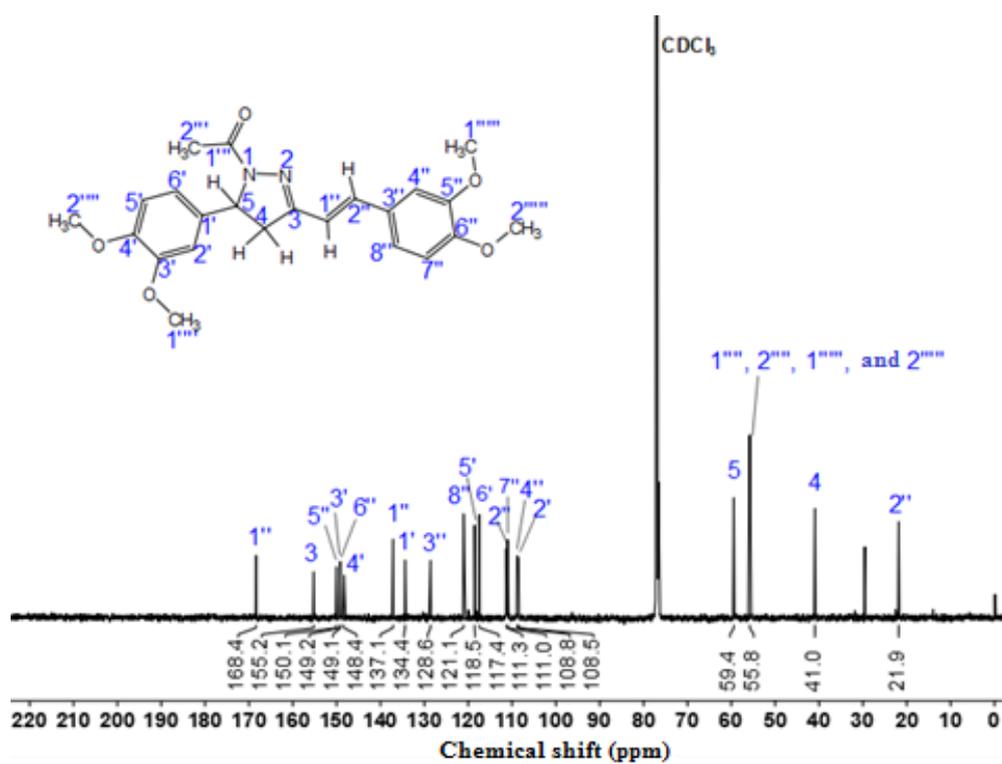
FIGURE S21. ^{13}C-NMR spectra of N-acetyl pyrazoline **3b**